



# Antioxidant Effect of Naringin Demonstrated Through a Bayes' Theorem Driven Multidisciplinary Approach Reveals its Prophylactic Potential as a Dietary Supplement for Ischemic Stroke

Manju Babu<sup>1</sup> · Rajas M. Rao<sup>2</sup> · Anju Babu<sup>3</sup> · Jenat Pazheparambil Jerom<sup>4</sup> · Anaekshi Gogoi<sup>1</sup> · Nikhil Singh<sup>1</sup> · Meenakshi Seshadri<sup>5</sup> · Animikh Ray<sup>6</sup> · Bhaskara P. Shelley<sup>7</sup> · Arnab Datta<sup>1,5</sup> 

Received: 31 January 2024 / Accepted: 23 September 2024

© The Author(s), under exclusive licence to Springer Science+Business Media, LLC, part of Springer Nature 2024

## Abstract

Naringin (NAR), a flavanone glycoside, occurs widely in citrus fruits, vegetables, and alcoholic beverages. Despite evidence of the neuroprotective effects of NAR on animal models of ischemic stroke, brain cell-type-specific data about the antioxidant efficacy of NAR and possible protein targets of such beneficial effects are limited. Here, we demonstrate the brain cell type-specific prophylactic role of NAR, an FDA-listed food additive, in an in vitro oxygen-glucose deprivation (OGD) model of cerebral ischemia using MTT and DCFDA assays. Using Bayes' theorem-based predictive model, we first ranked the top-10 protein targets (ALDH2, ACAT1, CTSD, FASN, LDHA, PTGS1, CTSD, LGALS1, TARDBP, and CDK1) from a curated list of 289 NAR-interacting proteins in neurons that might be mediating its antioxidant effect in the OGD model. When preincubated with NAR for 2 days, N2a and CTX-TNA2 cells could withstand up to 8 h of OGD without a noticeable decrease in cell viability. This cerebroprotective effect is partly mediated by reducing intracellular ROS production in the above two brain cell types. The antioxidant effect of NAR was comparable with the equimolar (50  $\mu$ M) concentration of clinically used ROS-scavenger and neuroprotective edaravone. Molecular docking of NAR with the top-10 protein targets from Bayes' analysis showed the lowest binding energy for CDK1 ( $-8.8$  kcal/M). Molecular dynamics simulation analysis showed that NAR acts by inhibiting CDK1 by stably occupying its ATP-binding cavity. Considering diet has been listed as a risk factor for stroke, NAR may be explored as a component of functional food for stroke or related neurological disorders.

**Keywords** Oxygen-glucose deprivation · Bioinformatics · Bayes' theorem · Molecular modeling · Astrocyte · CDK1

## Abbreviations

CDK1	Cyclin dependent kinase 1	EDV	Edaravone
DCFDA	2,-7,-Dichlorodihydrofluorescein diacetate	FBS	Fetal bovine serum
DMEM	Dulbecco's modified eagle medium	FDA	Food and Drug Administration
DMSO	Dimethyl sulfoxide	GO	Gene ontology
		GRAS	Generally recognized as safe

✉ Arnab Datta  
arnabdattaju@gmail.com; arnabdatta@yepopya.edu.in

<sup>1</sup> Laboratory of Translational Neuroscience, Division of Neuroscience, Yenepoya Research Center, Yenepoya (Deemed to be University), University Road, Deralakatte, Mangalore 575018, Karnataka, India

<sup>2</sup> Division of Data Analytics, Bioinformatics and Structural Biology, Yenepoya Research Center, Yenepoya (Deemed to be University), University Road, Deralakatte, Mangalore 575018, Karnataka, India

<sup>3</sup> Department of Biological Sciences, Indian Institute of Science Education and Research, Bhopal 462066, MP, India

<sup>4</sup> School of Biosciences, Mahatma Gandhi University, Kottayam 686560, Kerala, India

<sup>5</sup> Department of Pharmacology, Yenepoya Pharmacy College and Research Center, Naringana, Deralakatte, Mangalore 575018, Karnataka, India

<sup>6</sup> Father Muller Research Center, Father Muller Medical College, Mangalore 575002, Karnataka, India

<sup>7</sup> Department of Neurology, Yenepoya Medical College, Yenepoya (Deemed to be University), University Road, Deralakatte, Mangalore 575018, Karnataka, India

MCAO	Middle cerebral artery occlusion
MS	Mass spectrometry
MTT	3-(4,5-Dimethylthiazol-2-yl)-2,5-diphenyl tetrazolium bromide
NAR	Naringin
NGM	Normal growth medium
N2a	Neuro-2a
MD	Molecular dynamics
OGD	Oxygen glucose deprivation
ROS	Reactive oxygen species
RSA	Relative solvent accessibility
SD	Standard deviation

## Introduction

Dietary phytoconstituents such as flavonoids have been promoted as nutraceuticals for improving the general physiological and cognitive function of the brain to support healthy aging [1]. Naringin (NAR), a flavanone glycoside, occurs widely in vegetables, alcoholic beverages, and citrus fruits [2]. It is enlisted by the Food and Drug Administration (FDA) as a food additive under the “essential oil and/or oleoresin (solvent-free)” category and is *generally recognized as safe* (GRAS). To promote NAR as a component of functional food for stroke, which is the most common neurological disorder, preclinical data on the beneficial role of NAR in related physiological and pathological contexts is needed to plan for randomized clinical trials. Oxidative stress due to the generation of reactive oxygen species (ROS) and inflammation are common pathological mechanisms of aging and stroke [3]. Incorporating brain-healthy food with antioxidant and anti-inflammatory properties may help in reducing life-long dependence on prophylactic medications by favorably modifying common risk factors of stroke such as aging, hypertension, or diabetes. Scavenging of ROS has also been actively tested as a therapeutic approach during acute ischemic stroke with mixed results. Edaravone (EDV), the only neuroprotective drug that is approved for treating ischemic stroke patients in Japan and for amyotrophic lateral sclerosis by the FDA, is a free radical scavenger [4, 5].

NAR has shown protective effects in preclinical models of global [6], focal cerebral ischemia-reperfusion injury (e.g., in vivo middle cerebral artery occlusion (MCAO) model and in vitro oxygen-glucose deprivation (OGD) model) [7–9], and in an animal model of subarachnoid hemorrhage [10]. This protective effect is attributed to the anti-apoptotic, anti-inflammatory, anti-oxidative, or anti-nitrosative effects of NAR. Further, based on pharmacokinetic studies done on healthy rodents, NAR is reported to cross the blood-brain barrier [7].

Despite the encouraging findings of NAR on preclinical models of ischemic stroke, cell type-specific data about the

cerebroprotective and antioxidant efficacy of NAR on different brain cell types, such as astrocytes, are limited. None of the earlier studies promoted NAR as a dietary supplement and instead projected it as a potential therapeutic option for stroke [7, 9, 11]. Intriguingly, dietary risks feature ahead of high fasting plasma glucose and smoking among the 19 risk factors that contribute to stroke-related disability-adjusted life years in the *Global Burden of Disease Study 2019* [12]. This highlights the importance of an urgent implementation of diet-based primary prevention strategies with greater consumption of potentially functional foods to reduce the socioeconomic burden of stroke [13]. The FDA does not list NAR as an antioxidant or dietary supplement. Although different chemical databases enlist many interacting proteins of NAR with respect to a multitude of pharmacological effects in diverse pathophysiological settings, there is no data about direct protein targets of NAR in the context of ischemic stroke.

To this end, here we apply a multidisciplinary approach where cell-based experiments are interspaced by Bayes’ theorem-guided data integration and molecular modeling to show the prophylactic potential of NAR on cultured astrocytes and neurons in the in vitro OGD model of acute cerebral ischemia and possible mechanisms of the cerebroprotective action.

## Materials and Methods

### Chemicals and Reagents

All cell culture media, supplements, and Pluronic F-68 (PF68) were purchased from Himedia (Thane, Maharashtra, India) except fetal bovine serum (FBS), which was obtained from Gibco (Paisley, Scotland, UK). Details can be found in Supplemental Methods.

### External Data Sources and Bioinformatics Analysis

The following databases were explored for acquiring targets or interacting proteins of NAR: ChEMBL, Drug Gene Interaction Database, PubChem, etc. (Supplemental Methods). The structures of protein targets for docking were retrieved from the Research Collaboratory for Structural Bioinformatics Protein Data Bank (RCSB-PDB) and the AlphaFold Protein Structure Database. The conserved domain of proteins was retrieved from the InterPro database. The annotations of functional units in proteins were obtained from the Conserved Domain Database.

Target search was performed using filters like Target Organism—Homo sapiens, Rattus norvegicus, Mus musculus, and Target Type—Single Protein from the listed

databases in the external data sources (Supplemental Methods). The targets were presented as human gene symbols. Redundancies were removed from the final dataset.

The N2a RNA-Sequencing (RNA-Seq) dataset was obtained from the study by Skariah et al. [14], and the N2a proteomics datasets were downloaded from the PRIDE database using the keywords “Neuro-2a” and “N2a” [15]. The PRIDE projects with “.txt” search files from the MaxQuant (v2.1.3.0) search were retrieved. Out of these, the projects in which the proteomics data for the control N2a cell line were available were considered for the final analysis [16–20]. The various studies reporting proteomics responses of neurons following an OGD experiment were curated from our recently published systematic review on OGD-proteomics [21]. Protein targets that are annotated to ROS-related molecular function or biological process with direct experimental evidence were curated from the Gene Ontology (GO) database.

### Bayes’ Theorem for Large-Scale Data Integration and Sensitivity Analysis

Bayes’ theorem is a derivative of Bayesian statistics that takes into consideration the available knowledge about the parameters of a statistical model and updates it with the observed data. It uses the observational data as a likelihood function that determines the posterior distribution from the background knowledge, which is expressed as a prior distribution [22].

Bayes’ theorem can be formulated as

$$P(A|B) = \frac{P(B|A)}{P(B)}P(A) \quad (1)$$

where  $P(A|B)$  is the probability of  $A$  given  $B$  (posterior probability),  $P(B|A)$  is the probability of  $B$  given  $A$ ,  $P(A)$  is the prior probability for  $A$ , and  $P(B)$  is the sum of probabilities of  $B$  overall  $A$ . From a practical perspective,  $P(B|A)$  represents new experimental data being integrated at a given step after mapping it to probability (likelihood) values (range 0 to 1).

The complement of the minimum Bayes’ factor (cMBF) was calculated for an RNA-Seq dataset using the following formula.

$$\text{cMBF} = 1 - \exp\left[-(Z^*)^2/2\right] \quad (2)$$

where  $Z^*$  is the ratio of each value to the intrinsic noise in the measurement [23]. The intrinsic noise was determined by thresholding the experimental data obtained in the form of FPKM (fragments per kilo base of transcript per million) in the RNA-Seq dataset. The likelihood ( $P(B|A)$ ) was assigned from the cMBF values, and the posterior probability ( $P(A|B)$ ) was calculated using formula 1.

The objective of this predictive model was to rank the NAR protein targets that are likely to be responsible for its antioxidant effects in brain cells (e.g., neurons). Known protein targets of NAR were compiled from the different databases mentioned in the previous section and assigned an initial probability of  $1/n$  ( $n$  = total number of curated targets). A series of evidence-based datasets were introduced as likelihood function based on the following assumptions: the protein target must be (1) transcribed and (2) translated in the target brain cell type (i.e., neuron—N2a cells) to play a protective role following NAR administration, (3) the neuronal proteins that are perturbed following OGD stress are more likely to be involved directly or indirectly with the NAR effect, and (4) NAR is widely reported to have antioxidant effects in various diseases and in diverse contexts. The ROS-associated proteome is likely to mediate the antioxidant action of NAR in brain cells.

This model will rank these “ $n$ ” protein targets of NAR in a descending order of posterior probability in the cell line of interest (i.e., N2a cells). The Bayesian analysis underwent sensitivity testing using Spearman’s rank correlation ( $\rho$ ), which gives a nonparametric measure of the statistical dependence between two variables [22] (Supplemental Methods).

### Cell Culture

The mouse neuroblastoma cell line N2a (CCL-131) and rat type-1 astrocyte cell line CTX-TNA2 (CRL-2006) were purchased from the American Type Culture Collection (ATCC, VA, USA). Both cells were maintained in high-glucose Dulbecco’s Modified Eagle Medium (DMEM), supplemented with 10% FBS and 1% 100X antibiotic-antimycotic solution (10,000 U Penicilin, 10 mg Streptomycin, and 25  $\mu$ g Amphotericin B per ml in 0.9% normal saline) at 37 °C under humidified air containing 5% CO<sub>2</sub>. This medium will be referred to as normal growth medium (NGM). All experiments were performed between 4 and 15 passages of the cells.

### In Vitro OGD

The cells were seeded in 96 well plates in NGM for 24 h to achieve 60–70% confluency. After 24 h, the cells were subjected to differentiation by serum deprivation for 48 h in high-glucose DMEM. The differentiation media was replaced with glucose-pyruvate-free DMEM with 1% FBS (referred to as OGD media) that was deoxygenated using hypoxia gas (95% N<sub>2</sub>/5% CO<sub>2</sub>). The cells in the OGD media were then transferred to a humidified airtight hypoxia chamber (Stemcell Technologies, Vancouver, Canada) that was flushed with hypoxia gas, and the flow rate was maintained at 20 L/min for 5 min using Single Flow Meter (Stemcell).

The hypoxia chamber was incubated at 37 °C for different durations (4 – 24 h), while the normal cells in NGM (i.e., control) were incubated in the same incubator for identical durations [24].

### NAR and EDV Treatment

NAR was dissolved in dimethyl sulfoxide (DMSO) for the determination of the IC<sub>50</sub> value in cultured neuron cells. For efficacy studies, NAR-PF68 micelles were prepared using a thin-film hydration method as described earlier [25]. Briefly, NAR dissolved in methanol was evaporated using a rotary evaporator. The thin-film of NAR-PF68 was hydrated by deionized water via continuous stirring. The solution was filtered and finally lyophilized. Plain PF68 micelles without NAR were prepared using the same procedure and used as blank micelles. EDV (Neon Laboratories, Mumbai, India) was purchased as an injection solution (1.5 mg/mL) from a local pharmacy. It was used with an identical dosing regimen and concentration as NAR.

### MTT Assay

Metabolic activity was measured using the MTT assay [24]. After the treatment and OGD induction, brain cells were incubated for 1 h with MTT at a concentration of 0.5 mg/mL in DMEM medium at 37 °C. Formazan crystals were solubilized using DMSO. The absorbance was measured at 570 nm and reference at 700 nm using a Multiskan SkyHigh Microplate Spectrophotometer (Thermo Scientific, MA, USA).

### DCFDA Assay

Intracellular ROS formation was measured by 2', 7'-dichlorodihydrofluorescein diacetate (DCFDA) assay using 10 μM DCFDA with a loading time of 30 min [26]. The fluorescence was measured at an excitation and emission wavelength of 485 and 525 nm using the fluorescence microscope ZOE Fluorescent Cell Imager (Bio-Rad, CA, USA). The generation of ROS is proportional to the intensity of DCFDA. Hoechst (10 μM) was used to counterstain the nuclei. Hydrogen peroxide (200 μM) was used as a positive control to simulate oxidative stress on the brain cells. DCFDA positive cells and corrected total cell fluorescence (CTCF) were calculated using Image J software (v1.53u). The CTCF was calculated by measuring the area, integrated density, and mean grey value per cell considering multiple images of the same treatment group, and the resultant fluorescence was normalized by subtracting the background fluorescence of the image.

### Docking Studies and Analysis

NAR was docked to protein targets using the HADDOCK 2.4 web server [27]. The detailed docking protocol is provided in the Supplemental Methods. Subsequent analysis of the docked complexes was performed. The functionally relevant sites of the protein targets were searched on the InterPro web server and labeled on the respective protein structures. The functionally relevant sites were retrieved based on annotations in the Conserved Domain Database and visualized on the docked complex using the UCSF Chimera program (v1.17.3) [28].

### Molecular Dynamics (MD) Simulation and Analysis

The dynamics of the NAR-target protein complex were determined through a 100 ns MD simulation. The detailed methodology of MD simulation is described in Supplemental Methods. The visualizations of the MD trajectory were performed using the VMD program [29]. The frequency of hydrogen-bonded contacts was determined from the NAR-target protein complex trajectory, with each trajectory frame corresponding to 20 ps. The hydrogen bond frequency was calculated using the MDAnalysis program [30]. The solvent accessibility of functionally critical residues of the target protein was calculated by measuring the relative solvent accessibility (RSA) of the target protein residues involved in the formation of the NAR-target protein complex in the MD trajectory. RSA was calculated as the ratio of the absolute surface area of the residue in the protein and to the absolute accessible surface area of the residue in a GXG peptide, as calculated earlier [31]. The average of the absolute accessible-surface area of target protein residues in the MD trajectory was calculated using the gmxsasa tool of GROMACS (v2020.4). For comparison, the same calculations were performed for the experimental structure of the apo-form of the target protein.

### Statistical Analysis

Data were analyzed with GraphPad Prism (GraphPad Software, Inc., La Jolla, CA, USA) and IBM SPSS 27.0 Statistics software (SPSS Inc., NY, USA). All experiments and data analysis were performed at least in triplicate. The *n* value indicates the number of replicate readings, as mentioned in the respective figure legends. For fluorescent images, three fields were selected randomly for each condition, and the cells were counted by an analyst who was blinded to the group identity. The quantitative data are represented as the mean ± standard deviation (SD). A Shapiro-Wilk test was performed to check the normality of the data. One way analysis of variance (ANOVA) was used to determine statistical significance. Tukey's post hoc test was used for multiple

comparisons between different groups. Statistical significance was accepted at  $*P < 0.05$ ,  $**P < 0.01$ .

## Results

### Large-Scale Data Integration by Bayesian Predictive Model Shortlists NAR Targets in Neuron

We retrieved the mammalian gene symbols of known protein targets of NAR from nine different databases and compiled them after removing the duplicates to get a list of 289 protein targets, which was used to create a data vector of length 289. Of note, this list is bigger than any of the individual nine databases, such as ChEMBL, DGIdb, DTC, and TTD. To identify the proteins that are most likely to be responsible for the antioxidant effect of NAR under an OGD condition, we generated a Bayesian predictive model to rank these 289 proteins in descending order of probabilities. Mouse N2a cells were selected as an example cell line as it is one of the most common neuronal cell lines used for in vitro experiments on cerebral ischemia. The initial prior probability vector was assigned equal probabilities for all elements ( $P(A) = 1/289$ ) for an unbiased approach. We applied Bayes' theorem vector-wise twelve successive times (Fig. 1A, Bayesian pipel

ine), each time incorporating likelihood vectors representing a different omics data set to stratify these 289 protein targets (Supplemental Table 1). The first two steps assume that to be a target for NAR in the N2a cells, the protein must be expressed in the N2a cell line. For the RNA-Seq dataset, the bottom 10th percentile of FPKM was considered noise for the calculation of cMBF using Eq. (2). A high likelihood value ( $P = 0.95$ ) was assigned for the genes that are detected in the RNA-Seq dataset with a cMBF greater than 0.001. The genes that were not detected in the RNA-Seq dataset were assigned a likelihood value of 0.5 ( $P = 0.5$ ). Similarly, the proteins that were detected by mass spectrometry (MS) in large-scale proteomics experiments with at least one or more confident and unique peptides were assigned a likelihood value of 0.95. The proteins that were not detected by MS were not disfavored ( $P = 0.5$ ), keeping in mind the stochastic nature of data-dependent acquisition during MS analysis. One RNA-Seq dataset and six large-scale expression proteomics datasets were selected and individually integrated as the first seven Bayesian operations. The next four steps in the Bayesian model account for the proteins that are perturbed following OGD stress in different types of cultured neuron cells (i.e., HT22, SH-SY5Y, and B104) and for various time points. The ratio data (OGD/control) were retrieved and filtered using  $P$ -values and magnitudes that have been

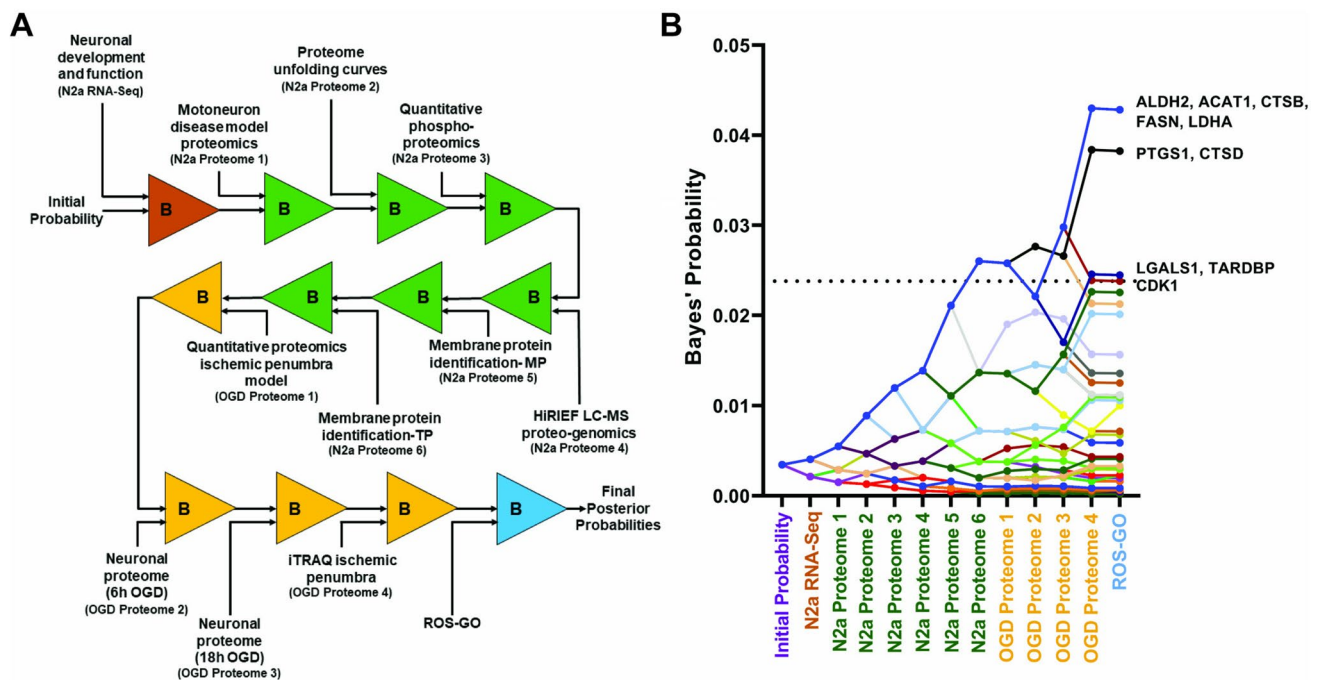


**Fig. 1** Bayesian predictive model. **A** Bayes' rule applied sequentially using RNA-Seq and proteomics data from different sources (as indicated), resulting in the identification of the most likely NAR targets. The Bayes' operators are color-coded rational-wise for easy visualization. Details of data sources are shown in Supplemental Table 1. **B**

Integration of RNA-Seq and diverse proteomics data yields a prioritized list of protein targets ranked by Bayes' probabilities. The dotted line marks the threshold for the top 10 protein targets. The x-axis is color-matched to the Bayes' operators. TP, total proteome; MP, membrane proteome

**Table 1** Most frequent hydrogen-bonded contacts between NAR and CDK1 residues observed in the MD simulation

Donor		Hydrogen		Acceptor		Frequency
Atom	Residue	Atom	Residue	Atom	Residue	
O7	NAR	H18	NAR	OD1	Asp86	0.379
O7	NAR	H18	NAR	OD2	Asp86	0.359
O8	NAR	H19	NAR	OD2	Asp86	0.343
O8	NAR	H19	NAR	OD1	Asp86	0.327
N	Asp86	HN	Asp86	O7	NAR	0.293
NE2	Gln132	HE22	Gln132	O7	NAR	0.086
O9	NAR	H20	NAR	O	Ile10	0.073
OG	Ser84	HG1	Ser84	O12	NAR	0.040
O5	NAR	H16	NAR	OE2	Glu8	0.040
NZ	Lys20	HZ1	Lys20	O10	NAR	0.039

decided by the authors in the respective studies to shortlist a protein as an OGD-perturbed protein. For the final step of the Bayesian analysis, we created a vector of 186 protein targets that are annotated to ROS-related molecular functions or biological processes in the GO database with direct experimental evidence. Details of the source datasets, the rationale for assigning a particular likelihood value to different target proteins, and Bayesian calculations are provided in Supplemental Spreadsheets A-B. Figure 1B shows the calculated posterior probabilities for all 289 NAR protein targets. Bayesian integration of multiple existing datasets resulted in the separation of a relatively small number of probable NAR targets from the 289 NAR-interacting proteins. The updated Bayesian ranking showed that among the top-10 NAR protein targets in N2a cells, mitochondrial aldehyde dehydrogenase, sterol O-acyltransferase 1, cathepsin B, fatty acid synthase, and lactate dehydrogenase A are the highest-ranked candidates, followed by prostaglandin-endoperoxide synthase 1, cathepsin D, galectin 1, TAR DNA binding protein, and cyclin dependent kinase 1 (CDK1) ([Ranked protein list](#)).

The Bayesian analysis underwent sensitivity tests using Spearman's rank correlation ( $\rho$ ) coefficient analysis. Twelve  $\rho$  values were obtained by removing each of the twelve datasets individually. These values ranged from 0.928 to 1.000, implying that no specific dataset had undue weight in creating the rankings (Supplemental Spreadsheet C-D). Furthermore, this analysis showed that the likelihood values assumed to calculate the posterior probability for a particular dataset did not have a critical impact on the overall analysis.

### Determination of $IC_{50}$ for OGD Model and NAR in Cultured Neuron

The above in silico results prompted us to experimentally test the effect of NAR on N2a cells in a suitable in vitro model of cerebral ischemia. OGD, which is the most common in vitro model of cerebral ischemia, was chosen [21].

To establish the in vitro OGD model, we exposed N2a cells in a glucose-pyruvate-deprived low-serum (1% FBS) media in a hypoxic environment for different durations spanning from 4 to 24 h. The OGD triggered a progressive reduction in the metabolic activity at 4, 8, 16, and 24 h compared to the N2a cells grown in NGM (Fig. 2A). There was about  $43 \pm 4\%$  ( $P < 0.01$ ) reduction in the metabolic activity after 8 h of OGD stress in N2a cells, as seen in the MTT assay. Based on this, 8 h OGD ( $IC_{50}$  for OGD stress) was further selected to study the efficacy of NAR in N2a cells.

We next tested the safety of NAR in cultured neuron cells by treating the differentiated N2a cells with different concentrations of NAR (0 – 2000  $\mu$ M in DMSO) or vehicle (DMSO) for 24 h. The cell viability did not show any reduction up to 1000  $\mu$ M concentration of NAR, as seen in the MTT assay (Supplemental Fig. 1). The  $IC_{50}$  of NAR was 1167  $\mu$ M. Based on this, 0 – 200  $\mu$ M of NAR was used for subsequent efficacy experiments.

### NAR Induces Metabolic Recovery and Scavenges ROS in Cultured Neuron Following OGD

To test the efficacy of NAR on the OGD model, the N2a cells were preincubated for 48 h with different concentrations of polymeric PF68-based micellar NAR (1, 10, 50, 100, 150, and 200  $\mu$ M) formulation or blank micelles that continued during 8 h of OGD. As shown in Fig. 2B, NAR induced a dose-dependent recovery of metabolic activity on the OGD-exposed cells at concentrations of 10  $\mu$ M ( $71 \pm 7\%$ ,  $P < 0.05$ ) and 50  $\mu$ M ( $95 \pm 4\%$ ,  $P < 0.01$ ) when compared with blank micelle-treated OGD-exposed cells. The neuroprotective effect had reached a plateau at higher doses (100 – 200  $\mu$ M). Therefore, we decided to test the ROS-scavenging effect of NAR using a concentration of 50  $\mu$ M.

ROS is one of the major contributing factors during the pathological evolution of ischemic stroke. Since NAR has shown ROS scavenging activity in the rodent MCAO model [7], we investigated the ROS production and its probable

reversal by NAR preincubation on the 8 h OGD model. We subjected the cells to DCFDA staining after 8 h of OGD stress (Fig. 2C). We found a significant increase in the percentage of DCFDA-positive cells (Fig. 2D) and fluorescence intensity (Fig. 2E) following 8 h OGD compared to the control (i.e., NGM,  $P < 0.01$ ). The OGD-induced oxidative injury was comparable to the damage caused by a 30-min treatment with 200  $\mu\text{M}$  hydrogen peroxide ( $\text{H}_2\text{O}_2$ ), which was used as a positive control to test the validity of the assay protocol. EDV (50  $\mu\text{M}$ ), which is in clinical use as a neuroprotective drug for ischemic stroke in Japan [4], was used as a standard ROS-scavenging agent and positive control to compare the relative efficacy with an equimolar concentration (i.e., 50  $\mu\text{M}$ ) of NAR. Both EDV and NAR-treated cells showed a reduction in the number of DCFDA-positive cells (EDV,  $95 \pm 1\%$ ,  $P < 0.01$ ; NAR,  $85 \pm 3\%$ ,  $P < 0.01$ ) and in the overall fluorescence intensity (EDV,  $91 \pm 2\%$ ,  $P < 0.01$ ; NAR,  $72 \pm 5\%$ ,  $P < 0.01$ ) compared to the blank micelle-treated cells after 8 h OGD. Overall, cultured neuron cells, when preincubated for 48 h with 50  $\mu\text{M}$  NAR, were able to withstand 8 h of OGD without a visible decrease in metabolic activity and a noticeable increase in the generation of ROS.

### NAR Induces Metabolic Recovery and Scavenges ROS in Type-1 Astrocyte Following OGD

Neurons and glia are present in roughly similar proportions in the human brain [32]. Astrocytes are the most abundant glial cell type [33]. It is known to support the neurons under normal physiological conditions and in pathological conditions such as ischemic stroke [34]. The encouraging results in N2a cells prompted us to test the metabolic and antioxidant efficacy of NAR on CTX-TNA2 cells, which are type-1 astrocyte cells.

We first determined the  $\text{IC}_{50}$  of OGD in CTX-TNA2 cells by exposing the astrocyte cells to different durations of OGD stress spanning from 4 to 24 h. Similar to N2a cells, CTX-TNA2 cells showed about a 50% ( $46 \pm 7\%$ ,  $P < 0.01$ ) reduction in metabolic activity after 8 h of OGD stress in the MTT assay (Fig. 3A). When different concentrations of NAR-PF68 (1, 10, 50, 100, 150, and 200  $\mu\text{M}$ ) formulation were preincubated for 48 h with astrocyte cells, we found a recovery of metabolic activity for the OGD-exposed cells at the concentrations of 10  $\mu\text{M}$  ( $72 \pm 3\%$ ,  $P < 0.05$ ) and 50  $\mu\text{M}$  ( $86 \pm 5\%$ ,  $P < 0.01$ ) when compared to blank micelle-treated 8 h OGD-exposed cells. The protective effect had reached a plateau at higher doses (100–200  $\mu\text{M}$ ) (Fig. 3B). In the DCFDA assay, we found a significant increase in the percentage of DCFDA-positive cells and fluorescence intensity following 8 h of OGD when compared to NGM (Fig. 3C–E). The NAR and EDV-treated cells showed a reduction in both the number of DCFDA-positive cells (NAR,  $83 \pm 5\%$ ,

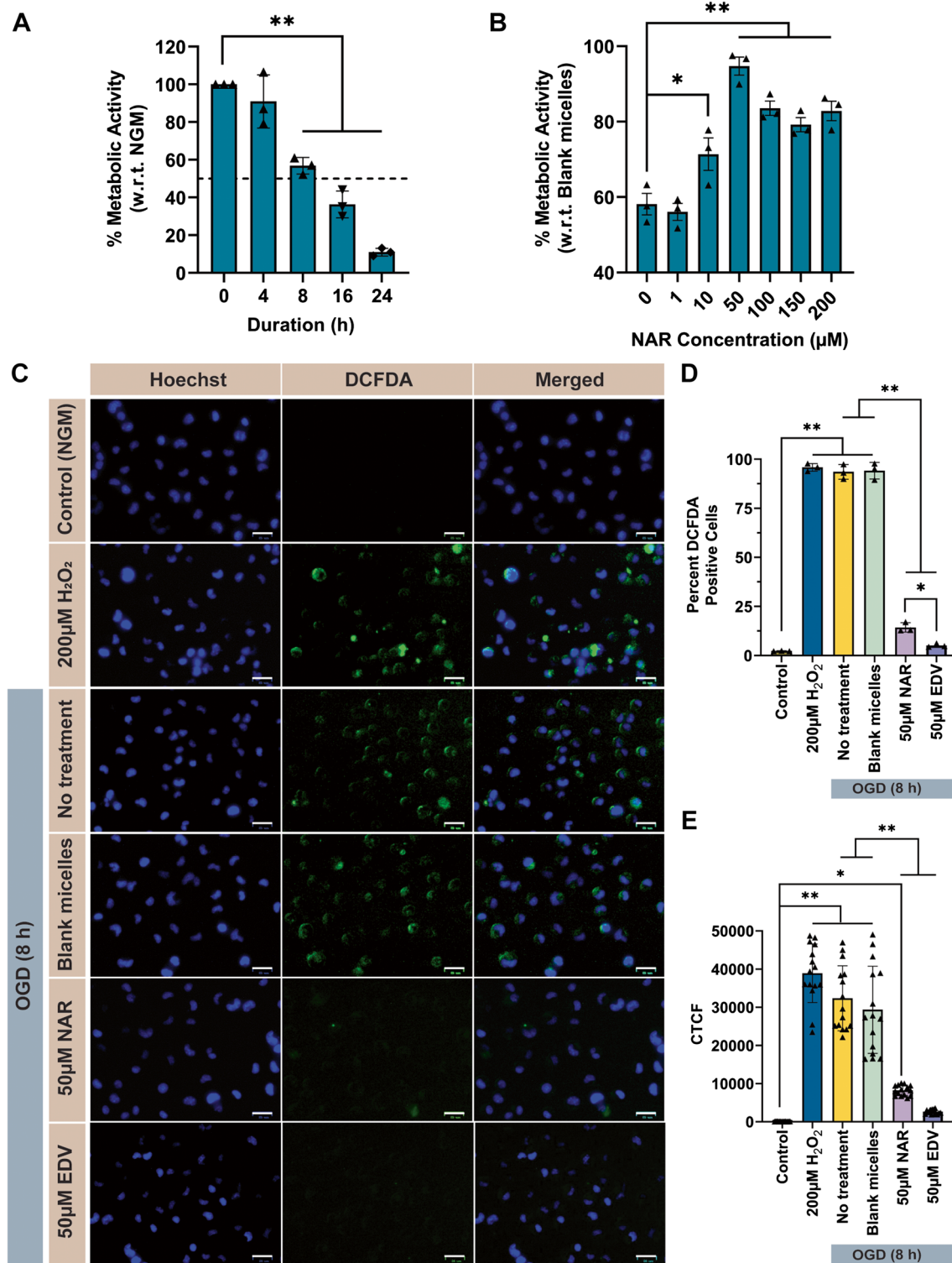
$P < 0.01$ ; EDV,  $85 \pm 2\%$ ,  $P < 0.01$ ) and overall fluorescence intensity (NAR,  $78 \pm 9\%$ ,  $P < 0.01$ ; EDV,  $94 \pm 4\%$ ,  $P < 0.01$ ) when compared to the blank micelle-treated 8 h OGD-exposed cells. EDV almost completely alleviated the OGD-induced generation of ROS in astrocyte cells. Although comparable, the ROS-scavenging effect of NAR was weaker in magnitude than equimolar concentrations of EDV.

Overall, the results show that the trends obtained from the MTT and DCFDA assays are similar for cultured neuron and type-1 astrocyte cells, while the magnitude of NAR-induced recovery following 8 h of OGD is higher for neurons compared to astrocytes. The preceding results provided experimental evidence about the favorable metabolic and antioxidant effects of NAR in the OGD model, while the Bayesian predictive model ranked the most probable protein targets of NAR that might be mediating these protective effects.

### Molecular Docking on Bayes'-Shortlist Identifies Direct NAR Target

To investigate if NAR produces its cerebroprotective effects by directly interacting with any of the top-ranked protein targets shortlisted from the Bayesian predictive model, virtual docking was performed between the top-10 protein targets and NAR. All ten targets were found to have low theoretical binding energy, ranging between  $-7$  and  $-9$  kcal/M (Supplemental Table 2) (Docked complexes). This approximately translates to a low inhibition constant of up to 5  $\mu\text{M}$  of NAR. Analysis of contacts between the NAR and the protein targets showed that the interactions are a combination of hydrophobic as well as hydrophilic contacts. Interestingly, much of the hydrophobic contacts were formed by the aromatic groups of NAR, while the hydrophilic contacts, largely involving hydrogen bonds, were formed by the saccharide groups (Supplemental Fig. 2). In most of the docked complexes, there was no spatial overlap between the NAR-target interface and functionally significant sites, such as substrate-binding/active sites, oligomerization sites, or protein-protein interaction interfaces (Supplemental Fig. 3).

Of the top 10 targets, NAR docked to CDK1 with the lowest binding energy of  $-8.9$  kcal/M. This translates to an inhibition constant of 330 nM, which is close to the drug-like binding affinity. Upon visualization of the binding interface, we found that the NAR-CDK1 interface significantly overlaps with the ATP-binding region of CDK1, in contrast with the other targets (Supplemental Fig. 3, Fig. 4A). A large part of the binding interface is formed by residues involved in ATP-binding, including the residues Gly11, Glu12, Phe82, Asp86, Lys89, Gln132, and Leu135 (Fig. 4B). The stability of the binding is contributed by the fact that NAR sits in the ATP-binding cavity [35], which is complementary to its shape.



From the 2D plot of NAR-CDK1 interactions, it is clear that the interface is dominated by hydrophobic contacts (Fig. 4C). In addition, the interface is further stabilized by a hydrogen bond between the residue Ser84 and the saccharide group of NAR. Interestingly, the interface is also

stabilized by a cation- $\pi$  interaction between the terminal aromatic group of NAR and the residue Lys9. The overlap of NAR binding with the ATP-binding site shows a potential inhibitory effect of NAR binding on CDK1 activity.



**Fig. 2** Measurement of metabolic activity and ROS production in differentiated N2a cells by MTT and DCFDA assays. **A** Time-dependent (0–24 h) percent metabolic activity in N2a cells post OGD by MTT assay,  $n=3$ . **B** Percent metabolic activity in N2a cells after pre- (48 h) and co-incubation (8 h) during OGD with different concentrations of NAR,  $n=3$ . **C** Fluorescence microscopic images of differentiated N2a cells in the DCFDA assay. The control cells were kept in normal growth media (NGM) without any treatment. A 30-min treatment with 200  $\mu\text{M}$   $\text{H}_2\text{O}_2$  was used as a positive control for showing the generation of green fluorescence in N2a cells. “No treatment” — Cells were exposed to 8 h OGD only. “Blank micelle” — Cells were pre- (48 h) and co-incubated (8 h) during OGD with PF68-based micellar formulation without NAR. An equimolar (50  $\mu\text{M}$ ) concentration of EDV was used as a positive control for showing the effective scavenging of ROS following 8 h OGD. Hoechst (10  $\mu\text{M}$ ) was used to counterstain the nuclei with blue fluorescence. Scale bar: 25  $\mu\text{m}$ , magnification: 200 $\times$ . **D** Quantification of DCFDA positive cells from randomly selected fields,  $n=3$ . **E** Quantification of CTCF,  $n=15$ . \* $P < 0.05$ , \*\* $P < 0.01$

### Molecular Dynamics Simulation Further Demonstrated Stable NAR-CDK1 Interactions

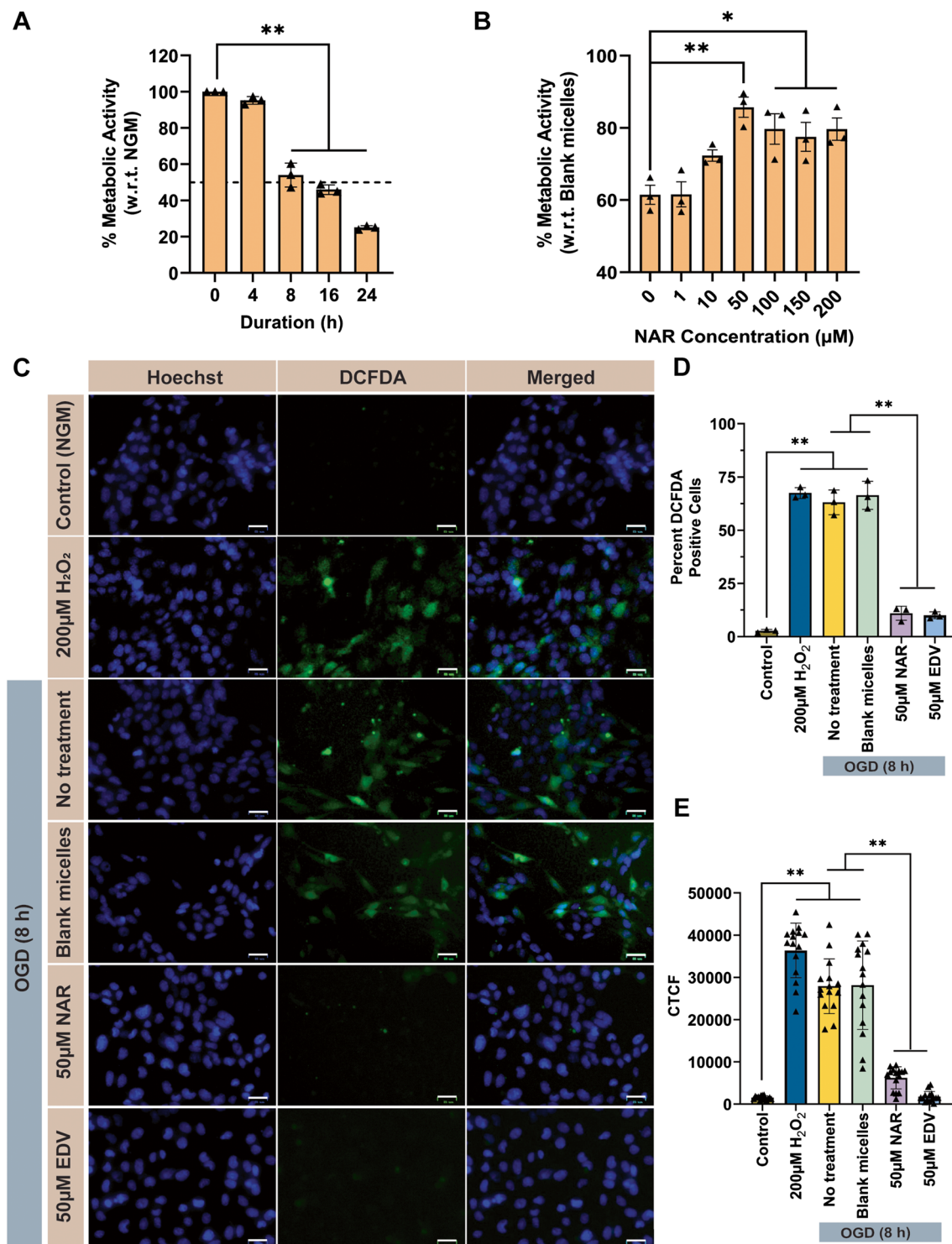
To assess the stability of the NAR-CDK1 complex, a short MD simulation was performed on the complex. The 100 ns MD simulation showed that NAR remained stably bound to the ATP-binding cavity of CDK1 (Fig. 4D, [NAR-CDK1 MD simulation](#)). However, the conformation of NAR and its relative orientation with respect to CDK1 changed during the simulation compared to its initial conformation. Interestingly, the flavone backbone (C6-C3-C6) remained exposed to the solvent in the simulation, contrary to the initial hypothesis that the hydrophobic character of this moiety may result in the group getting buried in the ATP-binding cavity (Fig. 4D). This could be due to the potential hydrogen bond formation between the water molecules and the hydroxyl groups present on the aromatic rings. While the flavone backbone was exposed to the solvent, the carbohydrate groups remained firmly bound to the ATP-binding cavity. We anticipate that the hydrogen bonds between the saccharide groups and polar or charged residues of the ATP-binding site may be the basis of the tight binding of NAR to CDK1. To test this, we calculated the frequency of hydrogen-bond contacts between NAR and protein atoms. Among the top 10 hydrogen-bonded contacts, three residues had the greatest contribution to the hydrogen-bonded interactions between NAR and CDK1. These include Asp86, Gln132, and Ser84 (Table 1). All these residues formed contacts with NAR during the docking experiments and formed hydrogen bonds with NAR during the simulation. The hydrogen-bonded contacts of particular interest are between the atoms comprising the side-chain carboxyl group of Asp86 and the atoms O7 and O8 of NAR. These contacts are the most frequently observed in the simulation, and they act as the anchor that holds NAR in the ATP-binding cavity (Table 1). To assess

if NAR binding has any impact on the solvent accessibility of ATP-binding residues, the RSA of critical ATP-binding residues was calculated. We compared the RSA values of the residues mentioned above with the RSA values of the same CDK1 residues from the experimental structure of the apo-form of CDK1 in complex with cyclin (PDB: 4YC6) [36]. Out of all the available residues in the ATP-binding cavity, we chose Phe82, Leu83, Ser84, and Lys89 as the most critical ATP-binding residues based on mutagenesis experiments evaluating the impact on inhibitor-binding activity [35]. Interestingly, we observed a global decline in the RSA of all the critical ATP-binding residues in the MD simulation. Of note, the RSA of Leu83 was reduced from 17.2 (apo-form of CDK1 structure) to 5.9 in our MD simulation (Table 2). Since an RSA value of 15 is considered to be the threshold below which an accessible residue is considered to be buried, Leu83 is clearly buried in our simulation. Similarly, Ser84 underwent a drastic reduction in RSA in the trajectory compared to its accessibility in the apo-form. Though the RSA value itself is 18.3, the high standard deviation suggests that the residue may be buried in numerous instances in the simulation (Table 2).

### Discussion

NAR is widely present in citrus fruits, wines, beers, vegetables, herbs such as rosemary, and plant species such as *Flemingia strobilifera* that are native to South, East, and South-east Asia [37]. In the Indian subcontinent and Myanmar, *F. strobilifera* is used in folkloric medicine to treat neurological and psychiatric disorders such as epilepsy and hysteria [38]. Rasam, a spice-rich and health-promoting food that is widely used in the South Indian diet, contains NAR [39]. Hence, a sizable population is exposed to NAR directly or indirectly, as it is consumed through regular food, as a component of functional food for general health benefits, or as traditional medicine. It can be hypothesized that the health benefits of these foods or plants are at least in part due to the presence of NAR. Hence, it is crucial to ascertain the beneficial effect of NAR and its possible molecular mechanism on various cell types of the brain. This will facilitate the optimal use of these food items in their natural form or when processed as functional food or nutraceuticals for preventing brain disorders such as ischemic stroke.

Our study, for the first time, demonstrated that NAR pre-incubation can promote metabolic recovery and scavenge ROS in an in vitro model of cerebral ischemia involving cultured rat astrocyte cells. The protective cellular effects are largely similar among neuron and astrocyte cell types, with minor differences in the magnitude of the effects. Of note, the favorable metabolic effect in the MTT assay showed a concentration-dependent increase only in the low



concentration range (i.e., 0 – 50  $\mu\text{M}$ , Figs. 2B, 3B). This confirms earlier reports that polyphenols such as genistein or epigallocatechin 3-gallate act as protective antioxidants in dietary physiological doses, whereas at higher concentrations, they may behave as pro-oxidants [40]. Interestingly, despite this low concentration, NAR showed a comparable yet modest antioxidant effect with equimolar concentrations

of clinically used neuroprotective EDV, which acts by scavenging ROS (Figs. 2C–E, 3C–E).

Earlier studies in animal and cell line models proposed NAR as a potential therapeutic agent or drug in the context of ischemic stroke [7, 9, 11]. However, NAR violates some of *Lipinski's rule of five* (mol weight > 500, hydrogen bond > 5, number of oxygen atoms > 10) on drug-likeness

**Fig. 3** Measurement of metabolic activity and ROS production in differentiated CTX-TNA2 cells by MTT and DCFDA assays. **A** Time-dependent (0–24 h) percent metabolic activity in differentiated CTX-TNA2 cells post OGD by MTT assay,  $n=3$ . **B** Percent metabolic activity in differentiated CTX-TNA2 cells after pre- (48 h) and co-incubation (8 h) during OGD with different concentration of NAR,  $n=3$ . **C** Fluorescence microscopic images of differentiated CTX-TNA2 cells in the DCFDA assay. The control cells were kept in normal growth media (NGM) without any treatment. A 30-min treatment with 200  $\mu\text{M}$   $\text{H}_2\text{O}_2$  was used as a positive control for showing the generation of green fluorescence in CTX-TNA2 cells. “No treatment” — Cells were exposed to 8 h OGD only. “Blank micelle” — Cells were pre- (48 h) and co-incubated (8 h) during OGD with PF68-based micellar formulation without NAR. An equimolar (50  $\mu\text{M}$ ) concentration of EDV was used as a positive control for showing the effective scavenging of ROS following 8 h OGD. Hoechst (10  $\mu\text{M}$ ) was used to counterstain the nuclei with blue fluorescence. Scale bar: 25  $\mu\text{m}$ , magnification: 200 $\times$ . **D** Quantification of DCFDA positive cells from randomly selected fields,  $n=3$ . **E** Quantification of CTCF,  $n=15$ . \* $P < 0.05$ , \*\* $P < 0.01$

that may adversely affect its pharmacokinetics [41]. NAR is structurally similar to several known pan-assay interference compounds, such as genistein and epigallocatechin gallate [42]. Also, the identification of 289 interacting proteins for NAR after curating different databases indicates the non-specific nature of NAR and target-protein interactions. These, along with the dismal record of chemically synthesized therapeutic agents in the past during numerous clinical trials on stroke, prompted us to consider naturally occurring NAR as a dietary supplement rather than a drug-hit conducive to therapeutic development. The GRAS status by the FDA for the use of NAR in food and carbonated beverages as a flavoring agent and also in the animal feed industry in formulations of personal care products and cosmetics further justifies detailed exploration of this bioflavonoid as a possible dietary supplement for stroke.

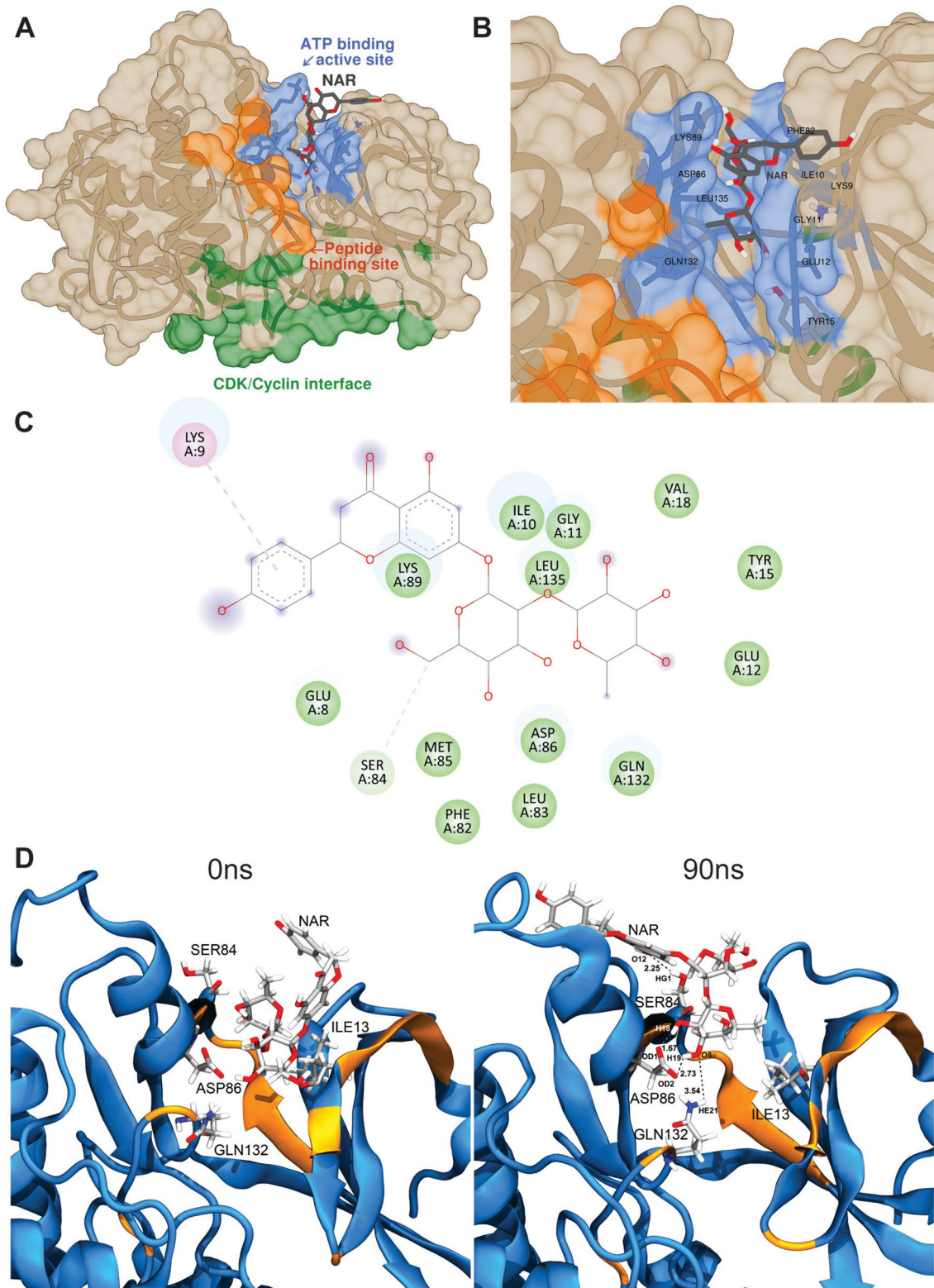
It is observed that although there are dedicated food databases that have compiled the composition, consumption, beneficial effects, and pharmacokinetics of bioactive substances from food (e.g., e-BASIS [43]) in general or focus on flavonoids (e.g., databases from the US Department of Agriculture [44]) or polyphenols (e.g., Phenol-Explorer [2]) in particular, none of these databases contain structural information related to protein-target interaction and molecular

dynamics of these complexes (Database links). It is known that most of the polyphenols or flavonoids are promiscuous molecules and interact with many proteins (e.g., 289 targets for NAR) [45]. Arguably, most of these interactions are indirect in nature. To the best of our knowledge, there is no easy way to determine the potential direct interactors among these targets. This makes any experimental (e.g., NMR or X-ray crystallography) or in silico (e.g., docking and MD simulation) structural study of all targets experimentally impossible or computationally challenging. The presence of only one protein complex in PDB for NAR (PDB: 8SFU), despite 289 known interacting proteins, is a testimony to the above-mentioned research gap [45]. Further, unless a proper context is introduced, virtual docking studies can be highly non-specific, as any small molecule can be computationally docked with any protein target [46]. We effectively tackled this caveat by applying Bayesian logic to introduce a reasonable context to the molecular modeling study. This addressed another long-standing research gap in the field of genomics and proteomics where, despite the accumulation of a large number of standalone big datasets generated by independent laboratories from the same preclinical model (e.g., in vitro OGD model [21]) or cell line (e.g., N2a) and from a comparable experimental setup, there was no easy way to retrieve useful information from these accumulated data. The Bayesian predictive model offered a rational solution by sequentially integrating one N2a RNA-Seq dataset, six N2a proteomics datasets, and four OGD-proteomics datasets along with ROS-linked proteome to shortlist the most likely protein targets of NAR that may be responsible for its anti-oxidative effect during OGD. Our Bayes' theorem-guided molecular modeling approach on NAR that is interspaced with cell-based assays offered a novel way of establishing the molecular mechanism of the beneficial effects of various naturally occurring bioactives with numerous interacting partners. This may assist in planning future randomized clinical trials on NAR as a dietary supplement to define it as a functional food.

It was observed that NAR can bind to the top-10 protein targets with low energies ranging between  $-7$  and  $-9$  kcal/M, with CDK1 being the target with the lowest binding energy (Supplemental Table 2). In the

**Table 2** Absolute and relative solvent accessible surface areas of ATP-binding CDK1 residues in the NAR-bound MD trajectory versus in the apo-form dimer with cyclin

Residue	Absolute solvent-accessible surface area from apo-form CDK1-cyclin complex(PDB: 4YC6) ( $\text{\AA}^2$ )	RSA from experimental structure	Average of absolute solvent-accessible surface area from MD( $\text{\AA}^2$ )	RSA from MD
Phe82	65.0	29.8	41.5 $\pm$ 0.1	19.0
Leu83	31.1	17.2	10.7 $\pm$ 0.1	5.9
Ser84	80.0	65.5	22.4 $\pm$ 15.1	18.3
Lys89	116.4	55.1	78.8 $\pm$ 16.1	37.3



remaining nine targets, NAR binds to regions other than the functionally significant regions, implying that NAR may not directly disrupt their functioning. It is possible that NAR may regulate them through long-range allosteric

communications. The other possibility could be that these targets are indirect targets of NAR. Notably, many of these targets, such as fatty acid synthase, galectin 1, and cathepsin D, have a known neuroprotective effect in stroke

**Fig. 4** Molecular docking and MD simulation analysis of NAR and CDK1. **A** A side-view of the NAR-CDK1 complex. Residues forming the interface with NAR are represented as sticks. Functionally significant residues, including ATP-binding site, peptide-binding site, and CDK/Cyclin interface are colored. **B** Top-view of the NAR-CDK1 complex zoomed-in to show the NAR-binding cavity. NAR is represented as sticks, colored according to the type of heteroatom. CDK1 residues forming contacts with NAR are represented as sticks and labeled. Visualization was performed using the UCSF Chimera program. **C** 2D contact map of NAR-CDK1 interactions. Residues forming hydrophobic contacts are represented as green spheres. Hydrogen bonds are represented as green colored dashed lines, and cation- $\pi$  interactions are represented as purple colored dashed lines. 2D contacts were plotted using the Discovery Studio Visualizer program (v21.1.0.20298). **D** Snapshots of the NAR-CDK1 complex at the beginning of MD simulation (left; time-point: 0 ns) and at the end of MD simulation (right; time-point: 90 ns). CDK1 is represented as blue cartoon, and the residues forming the ATP-binding site are represented as orange cartoon. NAR and residues forming frequent hydrogen-bonded interactions are represented as sticks. Atoms are colored based on the type (Hydrogen: white, Carbon: gray, Oxygen: red, Nitrogen: blue). The most frequent hydrogen-bonded contacts are represented as dashed lines between the hydrogen and the acceptor oxygen, along with respective distances (in Å). The atoms forming hydrogen bonds are labeled. Visualization was performed using the VMD program [29]

[47–49] (Supplemental Table 2). However, out of these ten docked targets, we are particularly interested in CDK1 for two reasons: (1) The NAR-CDK1 binding energy was translating to nanomolar-level affinity ( $-8.9$  kcal/M, with  $K_i$  of 330 nM), (2) CDK1 is the only target where NAR is directly bound to a functionally significant region, i.e., the ATP-binding site. This led us to hypothesize that NAR may directly inhibit CDK1 activity by binding to its ATP-binding site, which could be the molecular basis of the neuroprotective effect elicited upon NAR treatment to the cultured N2a cells. This hypothesis is consistent with the known CDK inhibitors such as Roscovitine and the semi-synthetic flavonoid Flavopiridol, which act by competitive inhibition of ATP-binding to CDK [50]. Considering the comparable MTT and DCFDA results between N2a and CTX-TNA2 cells (Figs. 2, 3) and our in-house proteomics results (data not shown) showing the presence of CDK1 protein in CTX-TNA2 cells, we anticipate a similar mechanism might apply to astrocytes as well. Of note, the astrocyte cell line, CTX-TNA2 could not be incorporated into the Bayesian model due to the unavailability of proteomics datasets on this cell line as well as a scarcity of OGD-proteomics data on astrocytes in general [21].

Finally, the MD simulation further showed that NAR binding to CDK1 is highly stable (Fig. 4D). The stability of the binding is largely contributed by the hydrogen-bonded interactions between the saccharide moiety of NAR with hydrophilic and charged residues of CDK1, such as Asp86, Gln132, and Ser84. Such interactions form the anchor that

fixes NAR to the ATP-binding cavity. As a result, the RSA of critical ATP-binding residues, which is a proxy for the accessibility of protein residues for various types of interactions, is reduced globally (Table 2). Since the ATP-binding residues are inaccessible for interaction with ATP, a lack of ATP-binding activity may eliminate the catalytic activity of CDK1. This could be the molecular mechanism through which NAR confers a cerebroprotective effect by inhibiting CDK1 activity.

In support of our hypothesis, experimental studies on CDK1 have demonstrated its role in stroke progression. In one study, 4 h OGD and 1 h MCAO induced neuronal death via activation of CDK1, which was partially reversed by genetic and pharmacological inhibition (R-roscovitine) of CDK1 [51]. Furthermore, the binding affinity of NAR for CDK1 is better compared to a well-characterized CDK inhibitor, R-roscovitine [52], and comparable to inhibitors such as p21 and hymenialdisine [53, 54]. It is possible that NAR may also target other CDK variants that share a high degree of structural homology with CDK1, such as CDK4 (ranked 15 in Bayes' shortlist) (Ranked protein list) and CDK5, both of which are proven to play a key role in neuronal death during stroke [55, 56]. Future proof-of-concept studies using genetic (e.g., CRISPR-Cas9 of CDK1) or pharmacological (e.g., CDK inhibition) approaches may provide valuable insights into the mechanism of the prophylactic effect of NAR in this OGD model.

## Conclusions

An interdisciplinary and novel approach was adopted, combining bioinformatics, Bayesian statistics, biochemical, and molecular modeling techniques to show the safety and prophylactic role of NAR against in vitro OGD. RNA-Seq and proteomics data from the N2a cell line, OGD model, and ROS-associated proteome were integrated using Bayes' theorem to rank likely protein targets of NAR responsible for its ROS-scavenging activity in the OGD model. The in silico predictive model was validated by demonstrating NAR's metabolic recovery-promoting and ROS-scavenging activity in N2a cells after 8 h of OGD, which was replicated in type-1 astrocyte CTX-TNA2 cells. These effects are comparable to equimolar concentrations of clinically used neuroprotective, EDV. Molecular modeling analysis showed that through its saccharide moiety, NAR forms a stable complex with the ATP-binding cavity of CDK1 and inhibits its enzymatic activity. Data generated from this study may encourage human intervention trials on NAR to validate its beneficial role as a prophylactic dietary supplement for stroke, aging, or other neurological disorders.

**Supplementary Information** The online version contains supplementary material available at <https://doi.org/10.1007/s12035-024-04525-6>.

**Acknowledgements** The authors thank Harikishore Amaravathi, and Deepthi Ann Thomas for helpful discussions, and Akash Mitra for helping with the docking analysis. The computational resources were provided by ROMEO-HPC of the University of Reims Champagne-Ardenne. The authors would like to thank Manuel Dauchez for his support with the computational resources.

**Author Contribution** Conceptualization and Supervision: Arnab Datta; Funding Acquisition: Arnab Datta, Rajas M. Rao; Wet-lab Experiments: Manju Babu, Jenat Pazheparambil Jerom, Anaekshi Gogoi, Nikhil Singh, Arnab Datta; In silico Bayes' Analysis: Arnab Datta, Manju Babu, Anju Babu; Molecular Modeling: Rajas M. Rao, Manju Babu; Data Analysis and Interpretation: Manju Babu, Rajas M. Rao, Animikh Ray, Meenakshi Seshadri, Bhaskara P. Shelley, Arnab Datta; Writing—Original Draft: Arnab Datta, Rajas M. Rao, Manju Babu. All authors edited and approved the final version of the manuscript.

**Funding** The study is funded by a DST-SERB Startup Research Grant (SRG/2021/001357 to Arnab Datta) and an institutional seed grant (YU/Seed Grant/092–2020 to Arnab Datta) at Yenepoya (Deemed to be University). Manju Babu is funded by a senior research fellowship under the guidance of Arnab Datta from ICMR (BMI/11(67)/2022). Rajas M. Rao is supported by an institutional seed grant (YU/Seed Grant/140–2023) at Yenepoya (Deemed to be University). Anaekshi Gogoi is funded by a junior research fellowship from DST-SERB Startup Research Grant (SRG/2021/001357 to Arnab Datta). The funders have no role in the design or implementation of the study.

**Data Availability** The raw simulation files have been deposited to zenodo, a general-purpose open repository developed under the European OpenAIRE program and operated by CERN (<https://doi.org/https://doi.org/10.5281/zenodo.8343461>). A web resource containing supplemental information is available at [https://yenepoya.res.in/database/LTN\\_Datta\\_Lab/Naringin-OGD/](https://yenepoya.res.in/database/LTN_Datta_Lab/Naringin-OGD/). This contains details of external databases for naringin protein targets, Bayes' Theorem, results of Bayes' Analysis, Docking, and MD simulation data with links to various food databases and PDB.

## Declarations

**Ethics Approval** This article does not contain any studies with human participants or animals performed by any of the authors.

**Consent to Participate** Not applicable.

**Consent for Publication** Not applicable.

**Competing Interests** The authors declare no competing interests.

## References

- Howes MR, Perry NSL, Vázquez-Londoño C, Perry EK (2020) Role of phytochemicals as nutraceuticals for cognitive functions affected in ageing. *Br J Pharmacol* 177(6):1294–1315. <https://doi.org/10.1111/bph.14898>
- Neveu V, Perez-Jiménez J, Vos F, Crespy V, du Chaffaut L, Mennen L, Knox C, Eisner R et al (2010) Phenol-Explorer: an online comprehensive database on polyphenol contents in foods. *Database (Oxford)* 2010:bap024. <https://doi.org/10.1093/database/bap024>
- Liguori I, Russo G, Curcio F, Bulli G, Aran L, Della-Morte D, Gargiulo G, Testa G, Cacciatore F, Bonaduce D, Abete P (2018) Oxidative stress, aging, and diseases. *Clin Interv Aging* 13:757–772. <https://doi.org/10.2147/CIA.S158513>
- Edaravone Acute Infarction Study G (2003) Effect of a novel free radical scavenger, edaravone (MCI-186), on acute brain infarction. Randomized, placebo-controlled, double-blind study at multicenters. *Cerebrovasc Dis* 15 (3):222–229. <https://doi.org/10.1159/000069318>
- Writing G, Edaravone ALSSG (2017) Safety and efficacy of edaravone in well defined patients with amyotrophic lateral sclerosis: a randomised, double-blind, placebo-controlled trial. *Lancet Neurol* 16(7):505–512. [https://doi.org/10.1016/S1474-4422\(17\)30115-1](https://doi.org/10.1016/S1474-4422(17)30115-1)
- Okuyama S, Yamamoto K, Mori H, Sawamoto A, Amakura Y, Yoshimura M, Tamanaha A, Ohkubo Y et al (2018) Neuroprotective effect of Citrus kawachiensis (Kawachi Bankan) peels, a rich source of naringin, against global cerebral ischemia/reperfusion injury in mice. *Biosci Biotechnol Biochem* 82(7):1216–1224. <https://doi.org/10.1080/09168451.2018.1456320>
- Feng J, Chen X, Lu S, Li W, Yang D, Su W, Wang X, Shen J (2018) Naringin attenuates cerebral ischemia-reperfusion injury through inhibiting peroxynitrite-mediated mitophagy activation. *Mol Neurobiol* 55(12):9029–9042. <https://doi.org/10.1007/s12035-018-1027-7>
- Yang J, Yuan L, Wen Y, Zhou H, Jiang W, Xu D, Wang M (2020) Protective effects of naringin in cerebral infarction and its molecular mechanism. *Med Sci Monit* 26:e918772. <https://doi.org/10.12659/msm.918772>
- Cao W, Feng SJ, Kan MC (2021) Naringin targets NFKB1 to alleviate oxygen-glucose deprivation/reoxygenation-induced injury in PC12 cells via modulating HIF-1alpha/AKT/mTOR-signaling pathway. *J Mol Neurosci* 71(1):101–111. <https://doi.org/10.1007/s12031-020-01630-8>
- Han Y, Su J, Liu X, Zhao Y, Wang C, Li X (2017) Naringin alleviates early brain injury after experimental subarachnoid hemorrhage by reducing oxidative stress and inhibiting apoptosis. *Brain Res Bull* 133:42–50. <https://doi.org/10.1016/j.brainresbull.2016.12.008>
- Gaur V, Aggarwal A, Kumar A (2009) Protective effect of naringin against ischemic reperfusion cerebral injury: possible neurobehavioral, biochemical and cellular alterations in rat brain. *Eur J Pharmacol* 616(1–3):147–154. <https://doi.org/10.1016/j.ejphar.2009.06.056>
- Collaborators GBDS (2021) Global, regional, and national burden of stroke and its risk factors, 1990–2019: a systematic analysis for the Global Burden of Disease Study 2019. *Lancet Neurol* 20(10):795–820. [https://doi.org/10.1016/S1474-4422\(21\)00252-0](https://doi.org/10.1016/S1474-4422(21)00252-0)
- Granato D, Barba FJ, Bursać Kovačević D, Lorenzo JM, Cruz AG, Putnik P (2020) Functional foods: product development, technological trends, efficacy testing, and safety. *Annu Rev Food Sci Technol* 11:93–118. <https://doi.org/10.1146/annurev-food-032519-051708>
- Skariah G, Seimetz J, Norsworthy M, Lannom MC, Kenny PJ, Elrakhawy M, Forsthoefel C, Drnevich J et al (2017) Mov10 suppresses retroelements and regulates neuronal development and function in the developing brain. *BMC Biol* 15(1):54. <https://doi.org/10.1186/s12915-017-0387-1>
- Perez-Riverol Y, Csordas A, Bai J, Bernal-Llinares M, Hewapathirana S, Kundu DJ, Inuganti A, Griss J et al (2019) The PRIDE database and related tools and resources in 2019: improving support for quantification data. *Nucleic Acids Res* 47(D1):D442–D450. <https://doi.org/10.1093/nar/gky1106>
- Hornburg D, Drepper C, Butter F, Meissner F, Sendtner M, Mann M (2014) Deep proteomic evaluation of primary and cell line

- motoneuron disease models delineates major differences in neuronal characteristics. *Mol Cell Proteomics* 13(12):3410–3420. <https://doi.org/10.1074/mcp.M113.037291>
17. Cox D, Ang CS, Nillegoda NB, Reid GE, Hatters DM (2022) Hidden information on protein function in censuses of proteome foldedness. *Nat Commun* 13(1):1992. <https://doi.org/10.1038/s41467-022-29661-2>
  18. Chen LL, Wang YB, Song JX, Deng WK, Lu JH, Ma LL, Yang CB, Li M et al (2017) Phosphoproteome-based kinase activity profiling reveals the critical role of MAP2K2 and PLK1 in neuronal autophagy. *Autophagy* 13(11):1969–1980. <https://doi.org/10.1080/15548627.2017.1371393>
  19. Branca RM, Orre LM, Johansson HJ, Granholm V, Huss M, Perez-Bercoff A, Forshed J, Kall L et al (2014) HiRIEF LC-MS enables deep proteome coverage and unbiased proteogenomics. *Nat Methods* 11(1):59–62. <https://doi.org/10.1038/nmeth.2732>
  20. Zhou Y, Gao J, Zhu H, Xu J, He H, Gu L, Wang H, Chen J et al (2018) Enhancing membrane protein identification using a simplified centrifugation and detergent-based membrane extraction approach. *Anal Chem* 90(4):2434–2439. <https://doi.org/10.1021/acs.analchem.7b03710>
  21. Babu M, Singh N, Datta A (2022) In vitro oxygen glucose deprivation model of ischemic stroke: a proteomics-driven systems biological perspective. *Mol Neurobiol* 59(4):2363–2377. <https://doi.org/10.1007/s12035-022-02745-2>
  22. Medvar B, Raghuram V, Pisitkun T, Sarkar A, Knepper MA (2016) Comprehensive database of human E3 ubiquitin ligases: application to aquaporin-2 regulation. *Physiol Genomics* 48(7):502–512. <https://doi.org/10.1152/physiolgenomics.00031.2016>
  23. Leo KT, Chou CL, Yang CR, Park E, Raghuram V, Knepper MA (2022) Bayesian analysis of dynamic phosphoproteomic data identifies protein kinases mediating GPCR responses. *Cell Commun Signal* 20(1):80. <https://doi.org/10.1186/s12964-022-00892-6>
  24. Datta A, Park JE, Li X, Zhang H, Ho ZS, Heese K, Lim SK, Tam JP et al (2010) Phenotyping of an in vitro model of ischemic penumbra by iTRAQ-based shotgun quantitative proteomics. *J Proteome Res* 9(1):472–484. <https://doi.org/10.1021/pr900829h>
  25. Mohamed EA, Abu H II, Yusif RM, Shaaban AAA, El-Sheakh AR, Hamed MF, Badria FAE (2018) Polymeric micelles for potentiated antiulcer and anticancer activities of naringin. *Int J Nanomedicine* 13:1009–1027. <https://doi.org/10.2147/ijn.S154325>
  26. Eruslanov E, Kusmartsev S (2010) Identification of ROS using oxidized DCFDA and flow-cytometry. *Methods Mol Biol* 594:57–72. [https://doi.org/10.1007/978-1-60761-411-1\\_4](https://doi.org/10.1007/978-1-60761-411-1_4)
  27. van Zundert GCP, Rodrigues J, Trellet M, Schmitz C, Kastiris PL, Karaca E, Melquiond ASJ, van Dijk M et al (2016) The HADDOCK2.2 web server: user-friendly integrative modeling of biomolecular complexes. *J Mol Biol* 428(4):720–725. <https://doi.org/10.1016/j.jmb.2015.09.014>
  28. Pettersen EF, Goddard TD, Huang CC, Couch GS, Greenblatt DM, Meng EC, Ferrin TE (2004) UCSF Chimera—a visualization system for exploratory research and analysis. *J Comput Chem* 25(13):1605–1612. <https://doi.org/10.1002/jcc.20084>
  29. Humphrey W, Dalke A, Schulten K (1996) VMD: visual molecular dynamics. *J Mol Graph* 14(1):33–38, 27–38. [https://doi.org/10.1016/0263-7855\(96\)00018-5](https://doi.org/10.1016/0263-7855(96)00018-5)
  30. Michaud-Agrawal N, Denning EJ, Woolf TB, Beckstein O (2011) MDAAnalysis: a toolkit for the analysis of molecular dynamics simulations. *J Comput Chem* 32(10):2319–2327. <https://doi.org/10.1002/jcc.21787>
  31. Miller S, Janin J, Lesk AM, Chothia C (1987) Interior and surface of monomeric proteins. *J Mol Biol* 196(3):641–656. [https://doi.org/10.1016/0022-2836\(87\)90038-6](https://doi.org/10.1016/0022-2836(87)90038-6)
  32. von Bartheld CS, Bahney J, Herculano-Houzel S (2016) The search for true numbers of neurons and glial cells in the human brain: a review of 150 years of cell counting. *J Comp Neurol* 524(18):3865–3895. <https://doi.org/10.1002/cne.24040>
  33. Endo F, Kasai A, Soto JS, Yu X, Qu Z, Hashimoto H, Gradinaru V, Kawaguchi R et al (2022) Molecular basis of astrocyte diversity and morphology across the CNS in health and disease. *Science* 378(6619):eadc9020. <https://doi.org/10.1126/science.adc9020>
  34. Patabendige A, Singh A, Jenkins S, Sen J, Chen R (2021) Astrocyte activation in neurovascular damage and repair following ischaemic stroke. *Int J Mol Sci* 22(8). <https://doi.org/10.3390/ijms22084280>
  35. Pratt DJ, Bentley J, Jewsbury P, Boyle FT, Endicott JA, Noble ME (2006) Dissecting the determinants of cyclin-dependent kinase 2 and cyclin-dependent kinase 4 inhibitor selectivity. *J Med Chem* 49(18):5470–5477. <https://doi.org/10.1021/jm060216x>
  36. Brown NR, Korolchuk S, Martin MP, Stanley WA, Moukhametzianov R, Noble MEM, Endicott JA (2015) CDK1 structures reveal conserved and unique features of the essential cell cycle CDK. *Nat Commun* 6:6769. <https://doi.org/10.1038/ncomms7769>
  37. Briguglio M, Hrelia S, Malaguti M, Serpe L, Canaparo R, Dell'Osso B, Galentino R, De Michele S et al (2018) Food bioactive compounds and their interference in drug pharmacokinetic/pharmacodynamic profiles. *Pharmaceutics* 10(4). <https://doi.org/10.3390/pharmaceutics10040277>
  38. Gahlot K, Lal VK, Jha S (2013) Anticonvulsant potential of ethanol extracts and their solvent partitioned fractions from Flemingia-strobilifera root. *Pharmacognosy Res* 5(4):265–270. <https://doi.org/10.4103/0974-8490.118825>
  39. Kalimuthu AK, Panneerselvam T, Pavada P, Pandian SRK, Sundar K, Murugesan S, Ammunje DN, Kumar S et al (2021) Pharmacoinformatics-based investigation of bioactive compounds of Rasam (South Indian recipe) against human cancer. *Sci Rep* 11(1):21488. <https://doi.org/10.1038/s41598-021-01008-9>
  40. Granato D, Mocan A, Câmara JS (2020) Is a higher ingestion of phenolic compounds the best dietary strategy? A scientific opinion on the deleterious effects of polyphenols in vivo. *Trends Food Sci Technol* 98:162–166. <https://doi.org/10.1016/j.tifs.2020.01.010>
  41. Lipinski CA, Lombardo F, Dominy BW, Feeney PJ (2001) Experimental and computational approaches to estimate solubility and permeability in drug discovery and development settings. *Adv Drug Deliv Rev* 46(1–3):3–26. [https://doi.org/10.1016/s0169-409x\(00\)00129-0](https://doi.org/10.1016/s0169-409x(00)00129-0)
  42. Baell J, Walters MA (2014) Chemistry: chemical con artists foil drug discovery. *Nature* 513(7519):481–483. <https://doi.org/10.1038/513481a>
  43. Plumb J, Pigat S, Bompola F, Cushen M, Pinchen H, Nørby E, Astley S, Lyons J et al (2017) eBASIS (bioactive substances in food information systems) and bioactive intakes: major updates of the bioactive compound composition and beneficial bioeffects database and the development of a probabilistic model to assess intakes in Europe. *Nutrients* 9(4). <https://doi.org/10.3390/nu9040320>
  44. Bhagwat SA, Haytowitz DB, Wasswa-Kintu SI, Pehrsson PR (2015) Process of formulating USDA's expanded flavonoid database for the assessment of dietary intakes: a new tool for epidemiological research. *Br J Nutr* 114(3):472–480. <https://doi.org/10.1017/s0007114515001580>
  45. Lacroix S, KlicicBadoux J, Scott-Boyer MP, Parolo S, Matone A, Priami C, Morine MJ, Kaput J et al (2018) A computationally driven analysis of the polyphenol-protein interactome. *Sci Rep* 8(1):2232. <https://doi.org/10.1038/s41598-018-20625-5>
  46. Chen YC (2015) Beware of docking! *Trends Pharmacol Sci* 36(2):78–95. <https://doi.org/10.1016/j.tips.2014.12.001>
  47. Janssen L, Ai X, Zheng X, Wei W, Caglayan AB, Kilic E, Wang YC, Hermann DM et al (2021) Inhibition of fatty acid synthesis

- aggravates brain injury, reduces blood-brain barrier integrity and impairs neurological recovery in a murine stroke model. *Front Cell Neurosci* 15:733973. <https://doi.org/10.3389/fncel.2021.733973>
48. Ishibashi S, Kuroiwa T, Sakaguchi M, Sun L, Kadoya T, Okano H, Mizusawa H (2007) Galectin-1 regulates neurogenesis in the subventricular zone and promotes functional recovery after stroke. *Exp Neurol* 207(2):302–313. <https://doi.org/10.1016/j.expneurol.2007.06.024>
  49. Hossain MI, Marcus JM, Lee JH, Garcia PL, Singh V, Shacka JJ, Zhang J, Gropen TI et al (2021) Restoration of CTSD (cathepsin D) and lysosomal function in stroke is neuroprotective. *Autophagy* 17(6):1330–1348. <https://doi.org/10.1080/15548627.2020.1761219>
  50. Vermeulen K, Van Bockstaele DR, Berneman ZN (2003) The cell cycle: a review of regulation, deregulation and therapeutic targets in cancer. *Cell Prolif* 36(3):131–149. <https://doi.org/10.1046/j.1365-2184.2003.00266.x>
  51. Marlier Q, Jibassia F, Verteneuil S, Linden J, Kaldis P, Meijer L, Nguyen L, Vandenbosch R et al (2018) Genetic and pharmacological inhibition of Cdk1 provides neuroprotection towards ischemic neuronal death. *Cell Death Discov* 4:43. <https://doi.org/10.1038/s41420-018-0044-7>
  52. De Azevedo WF, Leclerc S, Meijer L, Havlicek L, Strnad M, Kim SH (1997) Inhibition of cyclin-dependent kinases by purine analogues: crystal structure of human cdk2 complexed with roscovitine. *Eur J Biochem* 243(1–2):518–526. <https://doi.org/10.1111/j.1432-1033.1997.0518a.x>
  53. Harper JW, Elledge SJ, Keyomarsi K, Dynlacht B, Tsai LH, Zhang P, Dobrowolski S, Bai C et al (1995) Inhibition of cyclin-dependent kinases by p21. *Mol Biol Cell* 6(4):387–400. <https://doi.org/10.1091/mbc.6.4.387>
  54. Meijer L, Thunnissen AM, White AW, Garnier M, Nikolic M, Tsai LH, Walter J, Cleverley KE et al (2000) Inhibition of cyclin-dependent kinases, GSK-3beta and CK1 by hymenialdisine, a marine sponge constituent. *Chem Biol* 7(1):51–63. [https://doi.org/10.1016/s1074-5521\(00\)00063-6](https://doi.org/10.1016/s1074-5521(00)00063-6)
  55. Osuga H, Osuga S, Wang F, Fetni R, Hogan MJ, Slack RS, Hakim AM, Ikeda JE et al (2000) Cyclin-dependent kinases as a therapeutic target for stroke. *Proc Natl Acad Sci U S A* 97(18):10254–10259. <https://doi.org/10.1073/pnas.170144197>
  56. Tuo QZ, Liuyang ZY, Lei P, Yan X, Shentu YP, Liang JW, Zhou H, Pei L et al (2018) Zinc induces CDK5 activation and neuronal death through CDK5-Tyr15 phosphorylation in ischemic stroke. *Cell Death Dis* 9(9):870. <https://doi.org/10.1038/s41419-018-0929-7>

**Publisher's Note** Springer Nature remains neutral with regard to jurisdictional claims in published maps and institutional affiliations.

Springer Nature or its licensor (e.g. a society or other partner) holds exclusive rights to this article under a publishing agreement with the author(s) or other rightsholder(s); author self-archiving of the accepted manuscript version of this article is solely governed by the terms of such publishing agreement and applicable law.